

Title

A deep neural network predicts survival after heart imaging better than cardiologists

Authors

Alvaro Ulloa, MS^{ab}; Linyuan Jing, PhD^{ab}; Christopher W Good, DO^d;

David P vanMaanen, MS^{ab}; Sushravya Raghunath, PhD^{ab}; Jonathan D Suever, PhD^{ab};

Christopher D Nevius, BT^{ab}; Gregory J Wehner, PhD^c; Dustin Hartzel, BS^b; Joseph B Leader, BA^b; Amro Alsaïd, MBBCh^d; Aalpen A Patel, MD^e;

H Lester Kirchner, PhD^b; Christopher M Haggerty, PhD^{ab}; Brandon K Fornwalt, MD PhD^{abde}

^aDept of Imaging Science and Innovation, Geisinger, Danville, PA, United States

^bBiomedical and Translational Informatics Institute, Geisinger, Danville, PA, United States

^cDept of Biomedical Engineering, University of Kentucky, Lexington, KY, United States

^dHeart Institute, Geisinger, Danville, PA, United States

^eDept of Radiology, Geisinger, Danville, PA, United States

Summary

Predicting future clinical events, such as death, is an important task in medicine that helps physicians guide appropriate action. Neural networks have particular promise to assist with medical prediction tasks related to clinical imaging by learning patterns from large datasets. Significant advances have been made in predicting complex diagnoses from medical imaging¹⁻⁵. Predicting future events, then, is a natural but relatively unexplored extension of those efforts. Moreover, neural networks have not yet been applied to medical videos on a large scale, such as ultrasound of the heart (echocardiography). Here we show that a large dataset of 723,754 clinically-acquired echocardiographic videos (~45 million images) linked to longitudinal follow-

up data in 27,028 patients can be used to train a deep neural network to predict 1-year survival with good accuracy. We also demonstrate that prediction accuracy can be further improved by adding highly predictive clinical variables from the electronic health record. Finally, in a blinded, independent test set, the trained neural network was more accurate in discriminating 1-year survival outcomes than two expert cardiologists. These results therefore highlight the potential of neural networks to add new predictive power to clinical image interpretations.

Introduction

Cardiovascular disease is prevalent, costly, and responsible for a large proportion of morbidity and mortality worldwide.⁶ For example, approximately 1 in 3 deaths in the United States are attributable to cardiovascular disease, which amounts to more lives lost per year than cancer and chronic lower respiratory diseases combined. Cardiovascular disease is also the most common hospital discharge diagnosis and had an estimated global economic burden of \$863 billion in 2010⁷.

Imaging is critical to treatment decisions in cardiovascular medicine, with the most ubiquitous modality being ultrasound of the heart, or echocardiography. During a routine echocardiogram, approximately 10-50 videos (~3,000 images) are acquired to assess heart anatomy and function. In clinical practice, a cardiologist realistically has 10-20 minutes to interpret these 3,000 images within the context of numerous other data streams such as laboratory values, vital signs, additional imaging studies (radiography, magnetic resonance imaging, nuclear imaging, computed tomography) and other diagnostics (e.g. electrocardiogram). While these numerous and evolving sources of data offer the potential for more precise predictions, human capacity can only integrate limited amounts information.

Machine learning, and specifically deep neural networks (DNNs), can help unlock the predictive power from numerous sources of data by providing intelligent computer assistance to physicians. While DNNs have already shown incredible promise in the medical field, existing applications have focused almost entirely on diagnosing current problems¹, such as diabetic retinopathy², skin cancer³, pulmonary nodules⁴, cerebral microhemorrhage^{5,8}, and etiologies of left ventricular hypertrophy⁹. Predicting future events, then, is both a natural but relatively unexplored extension of those efforts and a task with added complexity where computers may add significant value. For example, a recent article in 216,221 patients showed how a Random Forest model can predict in-hospital mortality with high accuracy⁹. In cardiology, variables derived from the electronic health record have been used to predict 2-5 year all-cause mortality in patients undergoing coronary computed tomography^{10,11}, 5-year cardiovascular mortality in a general clinical population¹², and up to 5-year all-cause mortality in patients undergoing echocardiography¹³. However, none of these efforts have utilized DNNs to unlock the predictive power of the raw pixel data stored within the thousands of images in an echocardiogram.

Recent advances in DNN design have shown promising results in video-based prediction^{14,15}. We can now leverage this technology, in combination with large clinical imaging and electronic health record datasets, to generate clinically relevant predictions directly and automatically from the medical videos that make up an echocardiogram. In this paper, we show that a DNN can predict survival directly from echocardiographic videos with good accuracy, that this accuracy can be improved by incorporating additional clinical variables from the electronic health record, and that the DNN is more accurate in discriminating 1-year survival compared to

two Core Cardiovascular Training Statement (COCATS) Level III-trained physician echocardiographers.

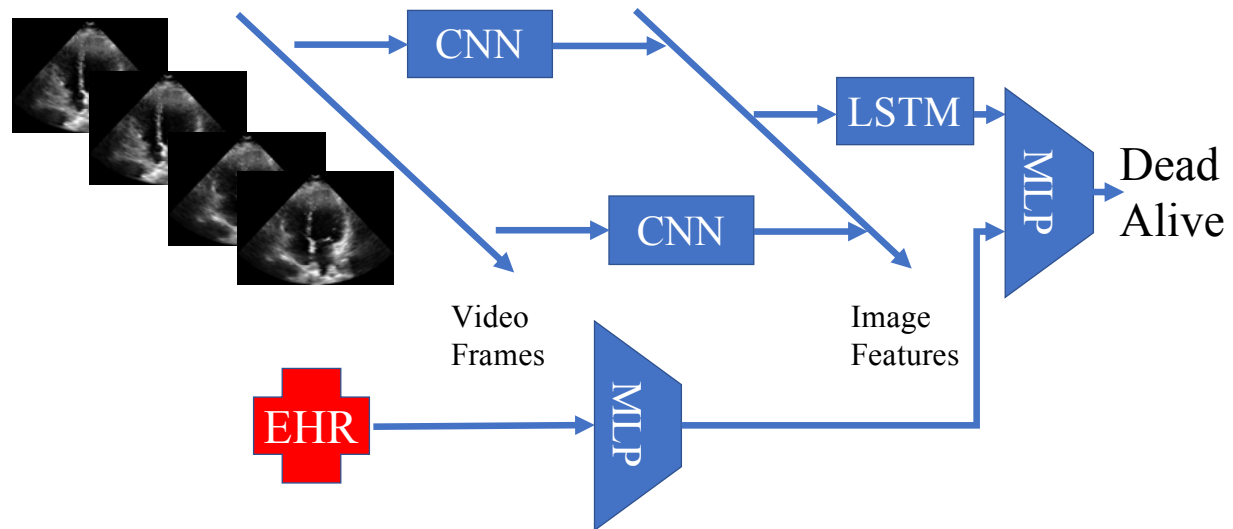


Figure 1: Neural network architecture for mortality prediction from echocardiography videos and electronic health record (EHR) data. CNN = convolutional neural network; LSTM = long short term memory; MLP = multilayer perceptron.

We utilize a time-distributed Convolutional Neural Network (CNN) with a Long Short Term Memory (LSTM) design in this work. CNNs are neural networks that exploit spatial coherence in an image to significantly reduce the number of parameters that a fully connected network would need to learn. CNNs have shown promise in image classification tasks¹⁶, even surpassing human abilities¹⁷. LSTMs are recurrent neural networks that learn from sequential (time-series) data^{18,19} and have achieved success in video captioning²⁰ and activity recognition from videos²¹. Details of the different model architectures attempted are described in the methods with the final architecture shown, see Figure 1. We first collated 723,754 echocardiographic videos from 27,028 patients that were linked to at least 1 year of longitudinal follow-up data to know

whether the patient was alive or dead within that time frame. The overall outcome distribution in this cohort was 16% deceased within a year after the study. This dataset consisted of approximately 45 million clinically-acquired echocardiography images. Based on a power calculation detailed in the methods, we separated data from 600 patients for a final test validation comparison against two independent cardiologists and used the remaining data for 5-fold cross-validation schemes.

During the acquisition of an echocardiogram, images of the heart and large blood vessels are acquired in different two-dimensional planes, or “views”, that are standardized according to clinical guidelines²². We generated separate models for each of 22 standard views and showed that the proposed models are able to accurately predict 1-year survival using only the raw pixel data as inputs. Specifically, the areas under the receiver operating characteristic curves (AUCs) ranged from 0.68-0.75, depending on the view (Figure 2). The highest performing model utilized the parasternal long axis (pl deep) view, which is typically reported by cardiologists as the most informative “summary” view of overall cardiac health since it contains elements of the left ventricle, left atrium, right ventricle, aortic and mitral valves, and whether or not there is a pericardial or left pleural effusion within a single view. These results were relatively insensitive to image resolution (no significant difference was observed between models using full native resolution images (400 x 600 pixels) and 4-fold down-sampled images (100 x 150 pixels); Extended Data Figure 3). Similarly, adding derived optical flow velocity maps²³ to the models along with the pixel level data did not improve prediction accuracy (Extended Data Figure 4).

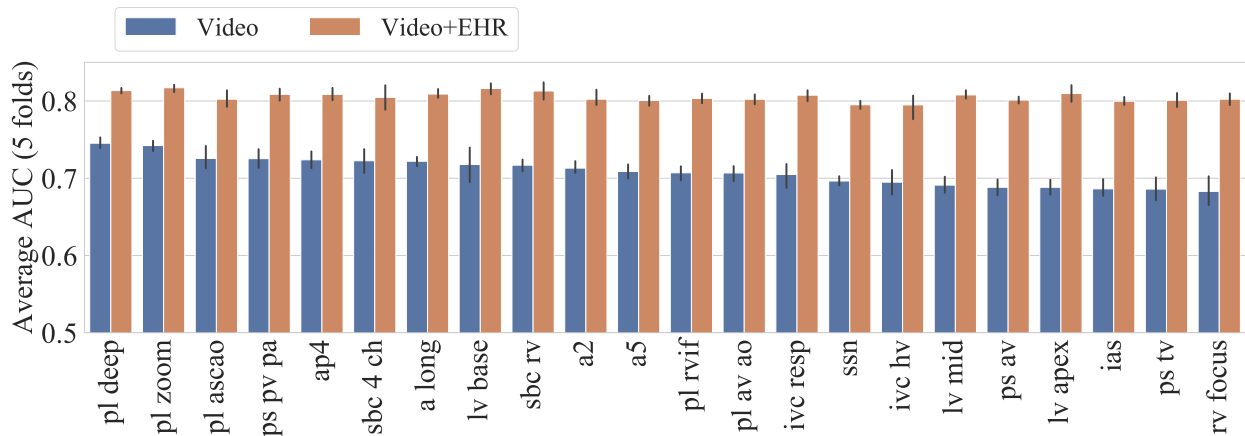


Figure 2: One-year mortality prediction performance ranking for all echocardiography views with video only (blue) and combined video plus 10 select clinical variables from the EHR (red). The error bars denote one standard deviation above and below the average across 5 folds.

We then added select clinical variables from each patient including age, tricuspid regurgitation maximum velocity, heart rate, low density lipoprotein [LDL], left ventricular ejection fraction, diastolic pressure, pulmonary artery acceleration time, systolic pressure, pulmonary artery acceleration slope, and diastolic function. These variables have previously been shown to contain >95% of the power for predicting 1-year survival in 171,510 patients¹³ and their addition improved accuracy to predict 1-year survival for all echocardiographic views (Figure 2), with AUCs ranging from 0.79-0.82.

Next we investigated the predictive accuracy of the models with the video input alone at additional survival intervals, including 3, 6, 9, and 12-month intervals after echocardiography. The models generally performed better at longer intervals, but AUCs for all cases were greater than 0.64, see Figure 3.

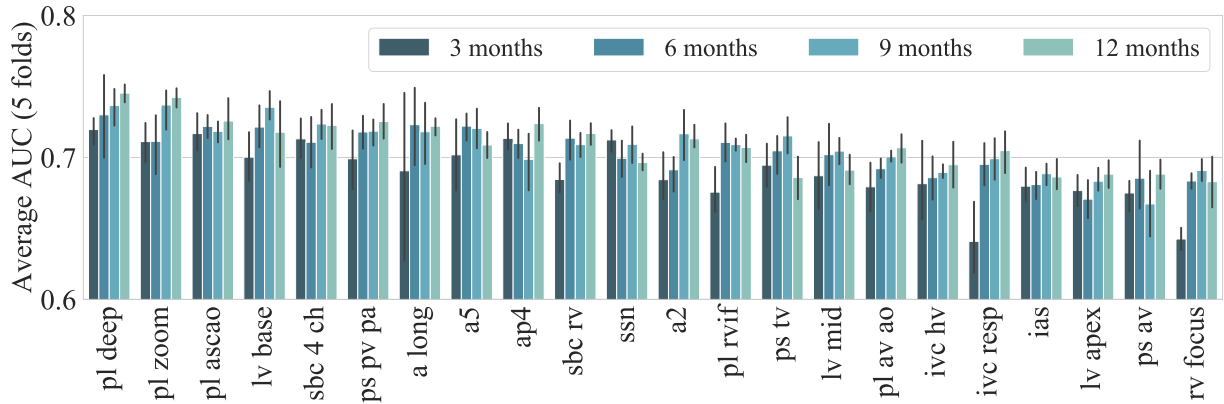


Figure 3: Mortality prediction performance for videos only at 3, 6, 9 and 12 months for all views.

The error bars denote one standard deviation above and below the average across 5 folds

We then developed a software platform (see Methods) that we used to display an echocardiographic video of interest along with the 10 select clinical EHR variables to two independent cardiologist echocardiographers who were blinded to the clinical outcomes. The cardiologists assessed whether each of 600 patients (independent test set extracted randomly from the original dataset of parasternal long axis views and not used for training of the machine) would be alive at one year based on the data presented. The final trained model (trained in all but these 600) was also applied to the same independent test set and found to have significantly higher accuracy compared to the cardiologists (both $p < 1e-6$), see Figure 4.

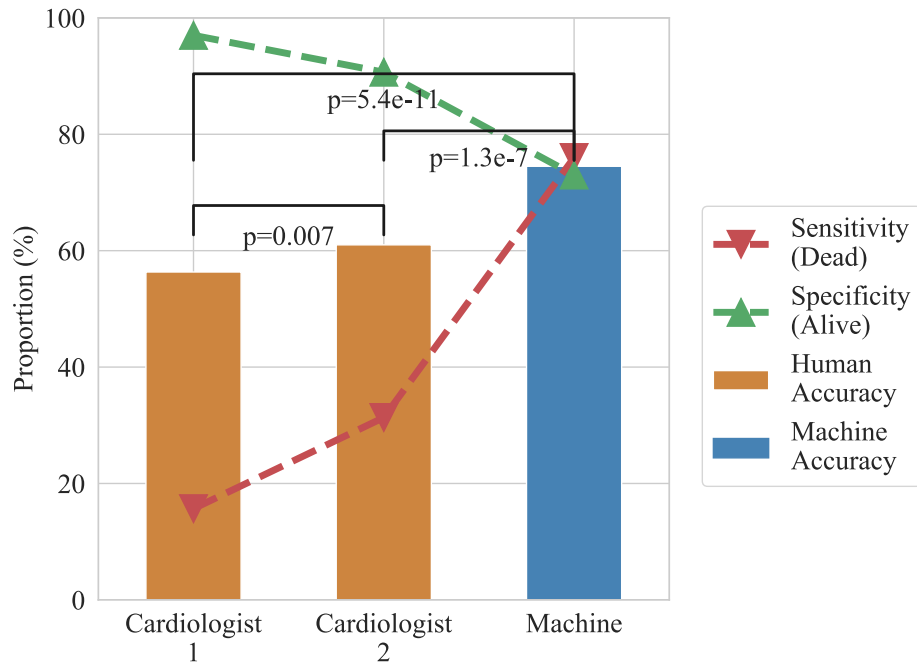


Figure 4: Cardiologists vs Machine performance for 1-year mortality prediction from the survey dataset of 600 samples with balanced prevalence.

Here we demonstrated the potential for DNNs to help cardiologists predict the survival of patients after echocardiography using both raw pixel data from videos and clinical data extracted from the electronic health record. For training the DNN, we leveraged ~723 thousand clinically-acquired videos of the heart consisting of ~45 million images. We showed that the ability of our DNN to discriminate 1-year survival surpassed that of trained cardiologists, suggesting that these models can add value beyond a standard clinical interpretation. We chose survival as a highly important, easily measured clinical outcome to demonstrate feasibility for this initial work. Further research will be needed to evaluate the performance of these models to predict additional clinically relevant outcomes in cardiology such as future hospitalizations or the need for major procedures such as a valve replacement. Though these data had inherent heterogeneity since they were derived from a large regional healthcare system with over 10 hospitals and hundreds of clinics, additional data

from other independent healthcare systems will be required to assess generalizability. Future work should be able to further improve accuracy by combining multiple videos into a single model, including Doppler based videos. Thus, methodology and architecture have been developed while feasibility and significant potential have been demonstrated for extracting predictive information from medical videos. With the ongoing rate of technological advancement and the rapid growth in electronic clinical datasets available for training, neural networks will augment future medical image interpretations with accurate predictions of clinical outcomes.

References

1. Quer, G., Muse, E. D., Nikzad, N., Topol, E. J. & Steinhubl, S. R. Augmenting diagnostic vision with AI. *Lancet* **390**, 221 (2017).
2. Gulshan, V. *et al.* Development and validation of a deep learning algorithm for detection of diabetic retinopathy in retinal fundus photographs. *JAMA* **316**, 2402–2410 (2016).
3. Esteva, A. *et al.* Dermatologist-level classification of skin cancer with deep neural networks. *Nature* **542**, 115–118 (2017).
4. Setio, A. A. A. *et al.* Pulmonary nodule detection in CT images: false positive reduction using multi-view convolutional networks. *IEEE Trans. Med. Imaging* **35**, 1160–1169 (2016).
5. Dou, Q. *et al.* Automatic detection of cerebral microbleeds from MR images via 3D convolutional neural networks. *IEEE Trans. Med. Imaging* **35**, 1182–1195 (2016).
6. Benjamin, E. J. *et al.* Heart Disease and Stroke Statistics—2017 Update: A Report From the American Heart Association. *Circulation* **135**, e146–e603 (2017).

7. Bloom DE, Cafiero ET, Jané-Llopis E, Abrahams-Gessel S, Bloom LR, Fathima S, Feigl AB, Gaziano T, Mowafi M, Pandya A, Prettner K, Rosenberg L, Seligman B, Stein AZ, W. C. The Global Economic Burden of Non-communicable Diseases. *Geneva, Switzerland: World Economic Forum* (2011).
8. Arbabshirani, M. R. *et al.* Advanced machine learning in action: identification of intracranial hemorrhage on computed tomography scans of the head with clinical workflow integration. *npj Digit. Med.* **1**, 9 (2018).
9. Rajkomar, A. *et al.* Scalable and accurate deep learning for electronic health records. *npj Digit. Med.* 1–10 (2018). doi:10.1038/s41746-018-0029-1
10. Motwani, M., Dey, D., Berman, D. S. & Et Al. Machine learning for prediction of all-cause mortality in patients with suspected coronary artery disease: a 5-year multicentre prospective registry analysis. *Eur. Heart J.* **52**, 468–476 (2016).
11. Hadamitzky, M. *et al.* Optimized prognostic score for coronary computed tomographic angiography: Results from the CONFIRM registry (COronary CT angiography evaluation for clinical outcomes: An international multicenter registry). *J. Am. Coll. Cardiol.* **62**, 468–476 (2013).
12. Kennedy, E. H., Wiitala, W. L., Hayward, R. A. & Sussman, J. B. Improved cardiovascular risk prediction using nonparametric regression and electronic health record data. *Med. Care* **51**, 251–8 (2013).
13. Samad, M. D. *et al.* Predicting Survival From Large Echocardiography and Electronic Health Record Datasets. *JACC. Cardiovasc. Imaging* (in press) (2018). doi:10.1016/j.jcmg.2018.04.026
14. Ji, S., Xu, W., Yang, M. & Yu, K. 3D Convolutional Neural Networks for Human Action

- Recognition. *IEEE Trans. Pattern Anal. Mach. Intell.* **35**, 221–231 (2013).
15. Karpathy, A. *et al.* Large-Scale Video Classification with Convolutional Neural Networks. in *2014 IEEE Conference on Computer Vision and Pattern Recognition* 1725–1732 (IEEE, 2014). doi:10.1109/CVPR.2014.223
 16. LeCun, Y. *et al.* Deep learning. *Nature* **521**, 436–444 (2015).
 17. He, K., Zhang, X., Ren, S. & Sun, J. Delving deep into rectifiers: Surpassing human-level performance on imagenet classification. *Proc. IEEE Int. Conf. Comput. Vis.* **2015 International Conference on Computer Vision, ICCV 2015**, 1026–1034 (2015).
 18. Hochreiter, S. & Schmidhuber, J. J. Long short-term memory. *Neural Comput.* **9**, 1–32 (1997).
 19. Greff, K., Srivastava, R. K., Koutnik, J., Steunebrink, B. R. & Schmidhuber, J. LSTM: A Search Space Odyssey. *IEEE Trans. Neural Networks Learn. Syst.* **28**, 2222–2232 (2017).
 20. Venugopalan, S. *et al.* Sequence to sequence - Video to text. *Proc. IEEE Int. Conf. Comput. Vis.* **2015 Inter**, 4534–4542 (2015).
 21. Donahue, J. *et al.* Long-Term Recurrent Convolutional Networks for Visual Recognition and Description. *IEEE Trans. Pattern Anal. Mach. Intell.* **39**, 677–691 (2017).
 22. Lang, R. M. *et al.* Recommendations for Cardiac Chamber Quantification by Echocardiography in Adults: An Update from the American Society of Echocardiography and the European Association of Cardiovascular Imaging. *J. Am. Soc. Echocardiogr.* **28**, 1–39.e14 (2015).
 23. Simonyan, K. & Zisserman, A. Two-Stream Convolutional Networks for Action Recognition in Videos. *arXiv Prepr. arXiv1406.2199* **9905**, 1–11 (2016).
 24. White, I. R., Royston, P. & Wood, A. M. Multiple imputation using chained equations:

- issues and guidance for practice. *Stat. Med.* **30**, 377–399 (2011).
25. Venugopalan, S. *et al.* Translating Videos to Natural Language Using Deep Recurrent Neural Networks. 1494–1504 (2014). doi:10.3115/v1/N15-1173
 26. Dauphin, Y. N., de Vries, H. & Bengio, Y. Equilibrated adaptive learning rates for non-convex optimization. in *Advances in Neural Information Processing Systems 28* 1504--1512 (2015). doi:10.1016/B978-0-12-385235-9.00003-5
 27. Duchi, J., Hazan, E. & Singer, Y. Adaptive subgradient methods for online learning and stochastic optimization. in *The Journal of Machine Learning Research* **12**, 2121–2159 (2011).

METHODS

Datasets and patients.

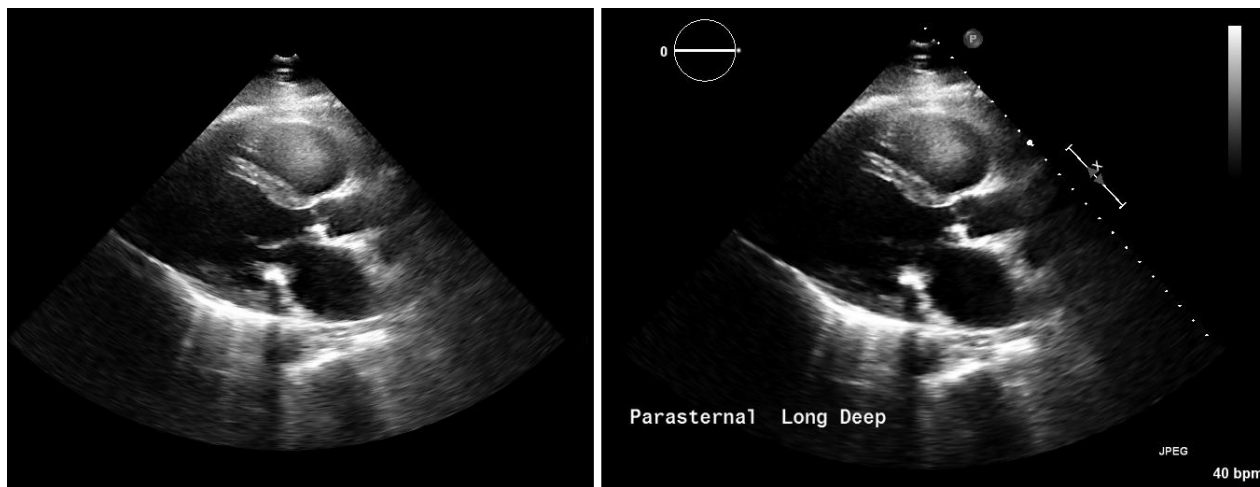
This retrospective study was approved by the Geisinger Institutional Review Board and was performed with a waiver of consent.

Image Collection and Preprocessing.

An echocardiography study consists of several videos containing multiple views of the heart. Two clinical databases, Philips iSite and Xcelera, contained all echocardiograms collected at Geisinger. We used DCM4CHEE (version 2.0.29) and AcuoMed (version 6.0) software to retrieve a DICOM file for each echocardiography video.

The retrieved DICOM files contained an annotated video and a raw video when the equipment was

configured to store it. The annotated video was stored in JPEG format with artificial markings on top of the raw video. The raw video contained only the beam-formed ultrasound image stored in a stream of bytes format (see Extended Data Figure 1). Without loss of generality, we used raw videos for all analyses. Learning from raw videos avoided potentially confounding features in the overlying artificial markings. Once a model is trained on raw videos, however, it could then be applied to annotated videos after preprocessing that removes the markings. Since the artificial markings on top of the raw video would be vendor dependent, the video preprocessing steps would be ad hoc designs.



Extended Data Figure 1: Examples of raw (left) and annotated (right) videos.

Using PyDICOM (version 1.0.2), we found that the raw video was stored in a DICOM element with code “(200D,3CF4)”. We transformed the stream of bytes to a sequence of frames by reading in little-endian byte order. The first two unsigned integers were interpreted as the total size and number of frames. For each frame, all but the first 16 bytes were uncompressed using the ZLIB software to produce a string of pixels for the image. We re-arranged the stream of pixels to form

frames with an approximately 2:3 row to column of pixels. The frame rate and dimensions were not documented or found in the DICOM tags. Thus, we calculated the total number of frames assuming that the annotated and raw videos spanned the same time duration. The frame dimensions were inferred by finding the integer combination of row and columns that provided the smoothest border of the image cone, as indicated by the number of times the first derivative of the row index of the first non-zero pixel sequence crossed zero. We linearly interpolated all raw videos to 30 frames per second.

Along with the pixel data, the DICOM file included tags that labelled the view as to which specific image orientation was acquired. These view tags had slight variations across studies for the same type of view. For example, an apical four chamber view could be tagged as “a4”, “a4 2d”, or “ap4”. We visually inspected samples of each unique tag and grouped them into 30 common views (Extended Data Table 1). We then cropped/padded each frame to the median dimensions among the view group.

Extended Data Table 1: View labels found in DICOM tags for the corresponding view type. The view tag in bold indicates the abbreviation used for the view type.

VIEW TYPE	VIEW TAG
APICAL 2	a2 , ap2 2d, a2 2d, a2 lavol, la 2ch
APICAL 3	a long , ap3 2d, a3 2d
APICAL 4	ap4 , ap4 2d, a4 2d, a4 zoom, a4 lavol, la ap4 ch

APICAL 4 FOCUSED TO RV	rv focus, rvfocus
APICAL 5	a5, ap5 2d, a5 2d
PARASTERNAL LONG AXIS	pl deep, psl deep
PARASTERNAL LONG ASCENDING AORTA	pl ascao, asc ao, pl asc ao
PARASTERNAL LONG MITRAL VALVE	pla mv
PARASTERNAL LONG PULMONIC VALVE	pl pv, pv lax
PARASTERNAL LONG RV INFLOW	pl rvif, rv inf, rvif 2d
PARASTERNAL LONG ZOOM AORTIC VALVE	pl av ao, av zoom
PARASTERNAL SHORT AORTIC VALVE	ps av, psavzoom, psax av
PARASTERNAL SHORT PULMONIC VALVE AND PULMONARY ARTERY	ps pv pa, ps pv, psax pv
PARASTERNAL SHORT TRICUSPID VALVE	ps tv, ps tv 2d, psax tv
SHORT AXIS APEX	sax apex
SHORT AXIS BASE	lv base
SHORT AXIS MID PAPILLARY	sax mid, sax
SUBCOSTAL 4CHAMBER	sbc 4 ch, sbc 4, sbc 4ch
SUBCOSTAL HEPATIC VEIN	ivc hv, sbc hv
SUBCOSTAL INTER-ATRIAL SEPTUM	ias, sbc ias, ias 2d

SUBCOSTAL IVC WITH RESPIRATION	ivc resp , sbc ivc, ivc insp, ivc snif, ivesniff, sniff
SUBCOSTAL RV	sbc rv
SUPRASTERNAL NOTCH	ssn , ssn sax
PARASTERNAL LONG ZOOM	pl zoom , psl, a4 scrn
PARASTERNAL LONG LAX	lax
SHORT AXIS MID PAPILLARY	lv mid
SHORT AXIS APEX	lv apex
APICAL 3 ZOOM	ap3
APICAL 2 ZOOM	ap2
SHORT AXIS BASE	sax base

We ultimately retrieved Philips-generated DICOM files with raw videos, view labels and at least one second duration.

Electronic health record data preprocessing.

Geisinger's EHR contained 594,862 echocardiogram studies from 272,280 unique patients performed over 19 years (February 1998 to September 2018). Each study included patient identifiers, date, and a findings report. We converted the study data into tabular format with 480 automatic and physician reported echocardiography measurements, vital sign measurements, and laboratory values.

We retrieved the closest (before or after) fasting LDL, HDL, blood pressure, heart rate, and weight measurements that were not taken at the time of the echocardiography study within a six-month window. When no measurement was available in that time window, we set the variable as missing.

All measurements were cleaned from physiologically out of limit values, which may be caused by input errors. In cases where no limits could be defined for a measurement, we removed extreme outliers that met two rules: 1) Value beyond the mean plus or minus three standard deviations and 2) Value below the 25th percentile minus 3 interquartile ranges or above the 75th percentile plus 3 interquartile ranges. The outlier values were set as missing.

Not all measurements were reported for all studies, however, the predictive models require all data to be complete. We imputed the missing data from continuous measurements in two steps. First, we conducted a time interpolation to fill in missing measurements using all available studies of an individual patient, i.e., missing values in between echocardiography sessions were linearly interpolated if complete values were found in the adjacent echocardiograms. Then, we kept 115 out of the 480 measurements because they were the most commonly measured with less than 90% missing values. This enabled us to conduct a robust Multiple Imputation by Chained Equations²⁴ (MICE).

After imputation of the continuous measurements, we imputed the missing diastolic function assessment by training a logistic regression classifier (One-vs-All) using 278,160 studies where diastolic function was known. We coded the reported diastolic function in an ordinal fashion with

-1 for normal, 0 for dysfunction (but no grade reported), and 1, 2 and 3 for diastolic dysfunction grades I, II, and III respectively.

We then selected the top ten 1-year survival predictors, as reported in a previous study¹³: Age (years), tricuspid regurgitation maximum velocity (cm/sec), left ventricular ejection fraction (%), pulmonary artery acceleration time (sec), pulmonary artery acceleration slope (cm/sec²), heart rate (beats per minute), diastolic function (normal, dysfunction but no grade reported, grade I, II or III), LDL (mg/DL) and diastolic and systolic blood pressures (mm[Hg]).

We calculated the patient's age and survival time from the date of the echocardiogram. The patient status (dead/alive) was based on the last known living encounter or confirmed death date, which is regularly checked against national databases in our system.

Data pruning.

The image collection and preprocessing resulted in 723,754 videos from 31,874 studies performed on 27,028 patients (an average of 22.7 videos per study). We linked the imaging and EHR data and discarded any imaging without EHR data. We then removed studies without enough follow up for a given survival experiment (3, 6, 9, and 12 months). Next, we kept studies that contained the required view and, because a single patient may have multiple echocardiographic studies in their lifetime, we randomly sampled one study per patient. This ensured that images from a single patient would not appear multiple times throughout training, validation, and testing groups.

We performed a sample size calculation using the Pearson Chi-square test which indicated that a

total of 600 (300 alive, 300 deceased) studies were needed to estimate and compare prognostic accuracy between the model and the two cardiologists. We assumed a 10% difference in accuracy between machine and cardiologist (80% vs 70%), 80% power, a significance level of 5%, and an approximate 40% discordancy. This was calculated using Power Analysis Software (PASS v15). Finally, we randomly sampled 600 studies for each view, as described by the sample size calculation, and set these aside from the valid samples to later compare the performance of the machine against two independent cardiologists. However, only the parasternal long axis view (representing the best performing model and the cardiologists' preference for the most comprehensive single view) was ultimately used for the cardiologist comparison. The total number of valid samples for each experiment and view is shown in Extended Data Table 2, and Extended Data Figure 2.

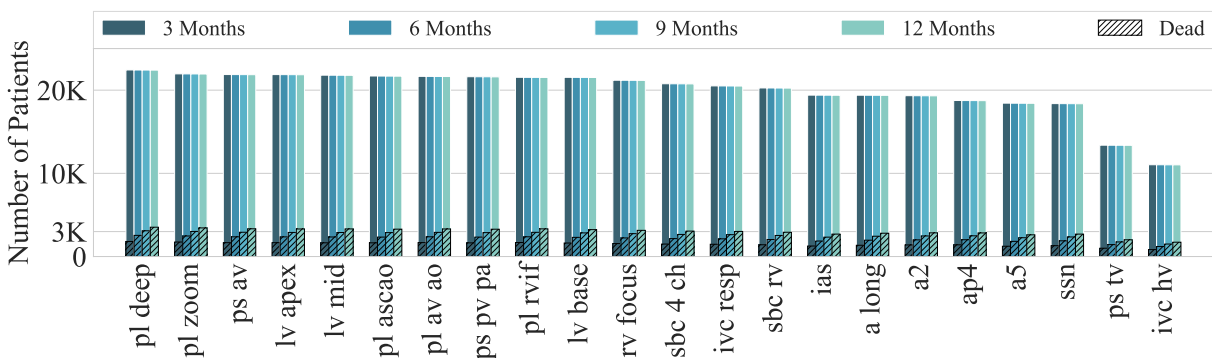
We excluded parasternal long mitral valve, parasternal long pulmonic valve, short axis apex zoom, short axis mid papillary zoom, parasternal long lax, apical 3 zoom, and apical 2 zoom views, as they did not have enough available samples to run the experiments.

Extended Data Table 2: Number of valid samples after setting 600 studies aside for the final test comparison to the 2 cardiologists.

VIEW GROUP	3	6	9	12
	MONTH	MONTH	MONTH	MONTHS
	S	S	S	
APICAL 2	19,334	19,328	19,323	19,316

APICAL 3	19,392	19,388	19,384	19,376
APICAL 4	18,755	18,749	18,745	18,737
APICAL 4 FOCUSED TO RV	21,192	21,186	21,181	21,173
APICAL 5	18,438	18,431	18,426	18,419
PARASTERNAL LONG AXIS	22,426	22,420	22,415	22,407
PARASTERNAL LONG ASCENDING AORTA	21,700	21,694	21,688	21,681
PARASTERNAL LONG RV INFLOW	21,544	21,538	21,534	21,528
PARASTERNAL LONG ZOOM	21,657	21,650	21,645	21,637
AORTIC VALVE				
PARASTERNAL SHORT AORTIC VALVE	21,875	21,870	21,865	21,857
PARASTERNAL SHORT PULMONIC VALVE AND PULMONARY ARTERY	21,614	21,609	21,605	21,596
PARASTERNAL SHORT TRICUSPID VALVE	13,385	13,379	13,375	13,370
SHORT AXIS BASE	21,541	21,535	21,530	21,523
SUBCOSTAL 4 CHAMBER	20,768	20,763	20,758	20,751
SUBCOSTAL HEPATIC VEIN	11,033	11,029	11,024	11,020
SUBCOSTAL INTER-ATRIAL SEPTUM	19,402	19,399	19,394	19,387

SUBCOSTAL IVC WITH RESPIRATION	20,510	20,505	20,499	20,492
SUBCOSTAL RV	20,263	20,259	20,254	20,247
SUPRASTERNAL NOTCH	18,382	18,378	18,372	18,365
PARASTERNAL LONG ZOOM	21,957	21,951	21,947	21,939
SHORT AXIS MID PAPILLARY	21,801	21,796	21,791	21,783
SHORT AXIS APEX	21,870	21,864	21,859	21,851



Extended Data Figure 2: Plot of the number of patients for experiments that required 3, 6, 9, and 12 months follow-up (as indicated in the Extended Data Table 2) with the proportion of dead patients (shaded bar).

Model selection.

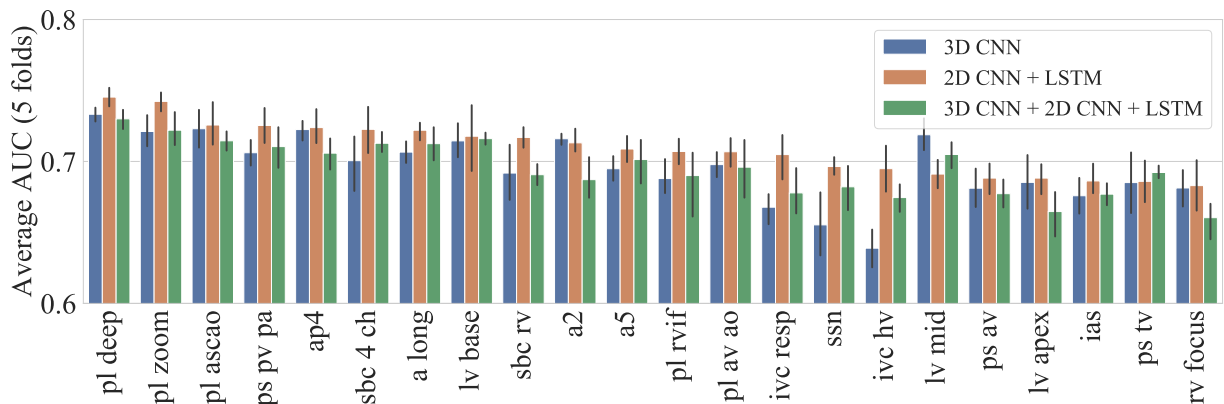
We implemented three different neural network architectures for video prediction: 3D Convolutional Neural Networks (CNN), time-distributed 2D CNNs with a Long Short-Term Memory (LSTM) coupling, and a mixture of 3D CNNs and 2D CNNs with an LSTM coupling.

Following the success of 3D CNNs for video classification¹⁴, we built 8 layers with kernel sizes of 5 and 3 for the first layer and size of 3 for the rest of the layers. We included a 2 x 3 x 3 pooling layer that reduced the output to a single maximum value every two layers. Following the CNN layers, the video features were flattened and passed through a 3-layer Perceptron classifier with rectified linear units (RELU) activations, 16 hidden units per layer and a sigmoid function at the final layer.

The second model, inspired from a sequence classification from CNN features²⁵, consisted of a time-distributed 2D CNN branch that trained on all frames of a video. This branch followed the same architecture as the first model but with 2D kernels. The output of the 2D CNN was then connected to an LSTM layer that accepted the CNN features for each frame as a time series multidimensional vector. The LSTM layer then returned a 16-dimensional vector that represented the entire sequence. Finally, we connected the LSTM output to the same 3-layer Perceptron as defined in the first model (see Figure 1).

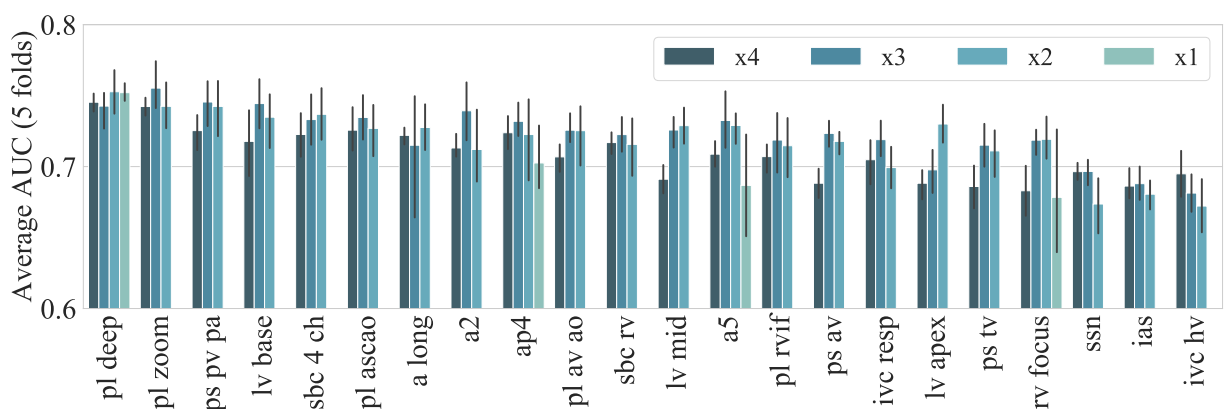
The third model combined the previous architectures with four 3D CNN layers and four subsequent 2D CNN layers with an LSTM layer, and the 3-layer perceptron for classification.

We evaluated the performance of these three models with a 5-fold cross-validation experiment on predicting 1-year survival from only the raw videos. Across all views, the second model showed better performance for most of the views (Extended Data Figure 3).



Extended Data Figure 3: One-year mortality prediction across all views with three different neural network architectures: a pure 3D CNN (blue), a 2D CNN with LSTM (orange), and a hybrid of the first two (green).

Similarly, we assessed the performance gain at different image resolutions. We down-sampled the videos by factors of 2, 3, and 4. No consistent significant gain in performance was observed across all views (Extended Data Figure 4). Thus, we decided to conduct all experiments with a down-sample factor of 4 to reduce computational cost.



Extended Data Figure 4: One-year mortality prediction across all views with different levels of down-sampling ranging from native (x1) to 4-fold (x4) down-sampling. Note that full native

resolution training was only done for select views due to the computational time required to complete the experiment at this resolution.

To incorporate EHR data into the prediction, we trained a three-layer MLP with 100, 10, and 10 hidden units. Then, we concatenated the last 10 hidden units with the LSTM output (16 hidden units) and fed its output to the same three-layer MLP used for video-only prediction.

Training algorithm.

We used the RMSProp²⁶ algorithm to train the networks with LSTM coupling, and AdaGrad²⁷ for the pure 3D CNN architecture. Each iteration of the 5-fold cross validation contained a training, validation, and test set. The training and test sets were sampled such that they had the same prevalence of alive patients, but the validation set was sampled with a balanced proportion. The validation set comprised of 10% of the training set.

As we trained the DNN, we evaluated the loss (binary cross-entropy) on the validation set at each epoch. If the validation loss did not decrease for more than 10 epochs we stopped the training and reported the performance, in AUC, of the test set. We set the maximum number of epochs to 1000 and kept the default training parameters as defined by the software Keras (version 2.2). Training always ended before the maximum number of epochs was reached.

Since the prevalence of each patient class is imbalanced (~16% deceased patients), we set the weights of each class as the total number of valid samples over two times the number of samples

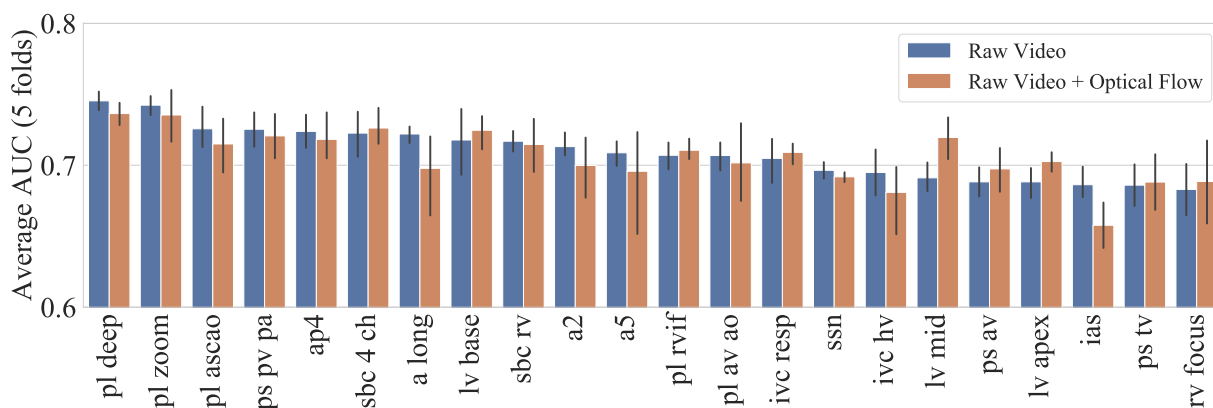
in each class. We also weighted each sample based on the actual time of survival. For example, when the patient survival was near 12 months, the patient sample was assigned a lower weight than when survival was close to 0 months. This was done to increase the influence of extremes in the model learning. We gave a weight of 5 to patients who survived 0 months after echocardiography, 0.1 for those who survived 12 months and 5 to those who survived more than 3 years. The weight for the patients in between was derived following two quadratic equations meeting at the study threshold, with 0.1 as the minimum.

All training was performed in an NVIDIA DGX1 platform. We independently fit each fold on each of the 8 available GPUs. The main experiment, shown in Figure 2, took a total of six days to complete.

Effect of adding optical flow inputs.

Optical flow velocity maps have been shown to be informative along with the original videos for classification tasks²³. Thus, we computed the dense optical flow vectors of the echocardiography raw videos using the Gunnar Farneback's algorithm as implemented in the OpenCV (version 2.4.13.7) software library. We set the pyramid scale to 0.5, the number of levels to 3, and the window size to 5 pixels. The vectors were then converted to color videos where the color indicated direction (as in the HSV color space) and the brightness denoted amplitude. This resulted in an image video that was fed to the neural network model through an independent 2D CNN with LSTM branch along with the raw video. As seen in Extended Data Figure 5, this combination of the optical flow video to the raw video did not yield consistently improved model performance compared with models using the raw video alone. Therefore, we did not use optical flow for the

final study analyses.

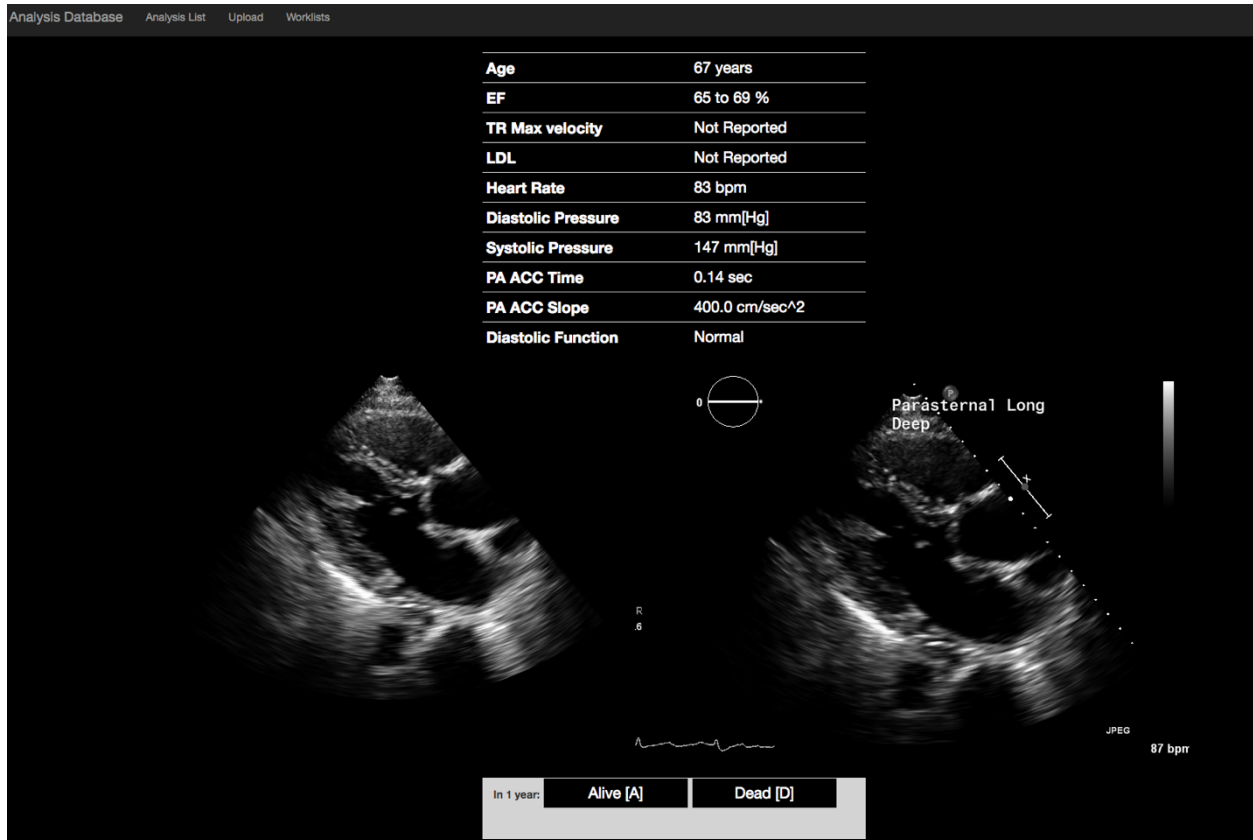


Extended Data Figure 5: One-year mortality prediction performance ranking for all echocardiography views using only the raw video (blue) versus the raw video with optical flow features (red).

Use of balanced outcomes in the cardiologist survey dataset. The 600-patient survey used to compare the accuracies of the cardiologists and the model, as described in the data pruning section, was intentionally balanced with respect to mortality outcomes (300 dead and 300 alive at one year) in order to ensure adequate power to detect differences in performance. The cardiologists were blinded to this distribution at the time of the review. We acknowledge that this balance is not reflective of typical clinical outcomes, particularly in a primary or secondary care setting, in which the base rate for 1-year survival is much higher. Hence, we cannot claim that this survey comparison between cardiologists and the model, as implemented, represents prediction in a realistic clinical setting. We do note, however, that the realistic clinical survival base rate was

represented in the model training sets, just as in the conditioning experiences of the cardiologists (consistent with their preference—high specificity for death—in over-estimating 1-year survival). Thus, the model was not advantaged in this regard by learning to expect this different outcome. Instead, rather than prediction informed by clinical base rates, our comparison sought to evaluate the true discriminative abilities and accuracies of the cardiologists compared to the machine.

Software for cardiologists survey. We deployed a web application with the interface shown in Extended Data Figure 6. The application required the cardiologist to input their institutional credentials for access. We showed the 10 EHR variables and the two versions of the video, raw and annotated. The application then recorded the cardiologist prediction as they clicked on either the “Alive” or “Dead” buttons.



Extended Data Figure 6: Interface of the web application developed for the cardiologist to predict survival one year after echocardiography.

Statistical analysis of comparison between Machine and Cardiologists. The cardiologists' response was binary, and the Machine's response was continuous. We set 0.5 as the threshold for the Machine's response prior to performing the final comparison experiment. Since all responses were recorded for the same samples, we conducted a Cochran's Q test to assess whether the three responses were significantly different in the proportion of correctly classified samples. This test showed that there was enough evidence that at least one of the responses was significantly different with a p-value of $1.8e-15$. A post hoc analysis of pairwise comparisons between the three responses resulted in Bonferroni-adjusted p-values of 0.007, $5.40e-11$, and $1.32e-07$ for the pairs Cardiologist

1 vs Cardiologist 2, Cardiologist 1 vs Machine, and Cardiologist 2 vs Machine, respectively.

Use of human subjects. This Human Subjects Research falls under Exemption 4 of the Health and Human Services human subject regulations since the research was conducted on existing patient data from the electronic health record at Geisinger.

Data availability statement. The medical training / validation data which were used for the current study are the property of Geisinger and are not publicly available due to the presence of patient identifiers. Some data may be available from the authors upon reasonable request and with permission from Geisinger.

Authors Contributions. A.U., C.H., and B.F conceived the study and designed the experiments. A.U. conducted all experiments. A.U. and S.R. wrote the software for applying deep learning to Echocardiography videos. A.U., L.J., D.V., D.H., J.S., and J.L. assembled the input data. L.K., G.W., and A.P. gave advice on experiment design. L.J., C.N., C.H., and B.F. manually audited the data for the cardiologist survey. C.G. and A.A. completed the survey. A.U. and B.F wrote the manuscript. All authors critically revised the manuscript.

Author Information. Reprints and permissions information is available at www.nature.com/reprints. No conflicts of interest were disclosed. Correspondence and requests for materials should be addressed to bkf@gatech.edu